Video Article

# Cardiac Magnetic Resonance Imaging at 7 Tesla

Daniel Stäb[1,2], Aiman Al Najjar[1], Kieran O'Brien[1,3], Wendy Strugnell[4], Jonathan Richer[3], Jan Rieger[5], Thoralf Niendorf[5], Markus Barth[1]

[1]The Centre for Advanced Imaging, The University of Queensland, Brisbane, Australia

[2]Department of Diagnostic and Interventional Radiology, University Clinic Würzburg, Würzburg, Germany

[3]Siemens Healthcare Pty Ltd, Brisbane, Australia

[4]Richard Slaughter Centre of Excellence in CVMRI, The Prince Charles Hospital, Brisbane, Australia

[5]MRI.Tools GmbH, Berlin, Germany

Correspondence to: Daniel Stäb at daniel.staeb@cai.uq.edu.au

URL: https://www.jove.com/video/55853
DOI: doi:10.3791/55853

Keywords: Cardiac, MRI, CINE, Cardiac Function, High Resolution, 7 Tesla, Ultrahigh field, Parallel Imaging, 32 channel coil, Shimming

Date Published: 7/13/2018

Citation: Stäb, D., Al Najjar, A., O'Brien, K., Strugnell, W., Richer, J., Rieger, J., Niendorf, T., Barth, M. Cardiac Magnetic Resonance Imaging at 7 Tesla. *J. Vis. Exp.* (), e55853, doi:10.3791/55853 (2018).

## Abstract

CMR at an ultra-high field (magnetic field strength $B_0 \geq 7$ Tesla) benefits from the signal-to-noise ratio (SNR) advantage inherent at higher magnetic field strengths and potentially provides improved signal contrast and spatial resolution. While promising results have been achieved, ultra-high field CMR is challenging due to energy deposition constraints and physical phenomena such as transmission field non-uniformities and magnetic field inhomogeneities. In addition, the magneto-hydrodynamic effect renders the synchronization of the data acquisition with the cardiac motion difficult. The challenges are currently addressed by explorations into novel magnetic resonance technology. If all impediments can be overcome, ultra-high field CMR may generate new opportunities for functional CMR, myocardial tissue characterization, microstructure imaging or metabolic imaging. Recognizing this potential, we show that multi-channel radio frequency (RF) coil technology tailored for CMR at 7 Tesla together with higher order $B_0$ shimming and a backup signal for cardiac triggering facilitates high fidelity functional CMR. With the proposed setup, cardiac chamber quantification can be accomplished in examination times similar to those achieved at lower field strengths. To share this experience and to support the dissemination of this expertise, this work describes our setup and protocol tailored for functional CMR at 7 Tesla.

## Video Link

The video component of this article can be found at https://www.jove.com/video/55853/

## Introduction

Cardiovascular magnetic resonance (CMR) is of proven clinical value with a growing range of clinical indications[1,2]. In particular, the evaluation of cardiac morphology and function is of major relevance and typically realized by tracking and visualizing the heart motion throughout the entire cardiac cycle using segmented breath-held two-dimensional (2D) cinematograpic (CINE) imaging techniques. While a high spatio-temporal resolution, high blood-myocardium contrast and high signal-to-noise ratio (SNR) are required, the data acquisition is highly constrained by the cardiac and respiratory motion and the use of multiple breath-holds as well as the need for whole heart or left-ventricular coverage often leads to extensive scan times. Parallel imaging, simultaneous multi-slice imaging or other acceleration techniques help to address the motion related constraints[3,4,5,6].

Moreover, to benefit from the inherent SNR gain at higher magnetic fields, high field systems with $B_0 = 3$ Tesla are increasingly employed in clinical routine[7,8]. The development has also encouraged investigations into ultra-high field ($B_0 \geq 7$ Tesla, $f \geq 298$ MHz) CMR[9,10,11,12,13,14]. The gain in SNR and blood-myocardium contrast inherent to the higher field strength holds the promise to be transferrable into enhanced functional CMR using a spatial resolution that exceeds today's limits[15,16,17]. In turn, new possibilities for magnetic resonance (MR) based myocardial tissue characterization, metabolic imaging and microstructure imaging are expected[13]. So far, several groups have demonstrated the feasibility of CMR at 7 Tesla and specifically tailored ultra-high field technology has been introduced[17,18,19,20,21,22]. Regarding these promising developments, the potential of ultra-high field CMR can be considered to be yet untapped[13]. At the same time, physical phenomena and practical obstacles such as magnetic field inhomogeneities, radio frequency (RF) excitation field non-uniformities, off-resonance artifacts, dielectric effects, localized tissue heating and field strength independent RF power deposition constraints make imaging at ultra-high field challenging[10,17]. The latter are employed to control RF induced tissue heating and to ensure safe operation. Moreover, electrocardiogram (ECG) based triggering can be significantly impacted by the magneto-hydrodynamic (MHD) effect[19,23,24]. To address the challenges induced by the short wavelength in tissue, many-element transceiver RF coil arrays tailored for CMR at 7 Tesla were proposed[21,25,26,27]. Parallel RF transmission provides means for transmission field shaping, also known as $B_1$+ shimming, which allows to reduce the magnetic field inhomogeneities and susceptibility artefacts[18,28]. While at the current stage, some of these measures might increase the experimental complexity, the concepts have proven helpful and may be translated to the clinical field strengths of CMR 1.5 T or 3 T.

Currently, 2D balanced steady state free precession (bSSFP) CINE imaging is the standard of reference for clinical functional CMR at 1.5 T and 3 T[1]. Recently, the sequence was successfully employed at 7 Tesla, but a large number of challenges remain[19]. Patient specific $B_1^+$

 

shimming and extra RF coil adjustments were applied to manage RF power deposition constraints and careful $B_0$ shimming was performed to control the sequence typical banding artifacts. With an average scan time of 93 minutes for left-ventricular (LV) function assessment, the efforts prolonged the examination times beyond clinically acceptable limits. Here, spoiled gradient echo sequences provide a viable alternative. At 7 Tesla, total examination times of (29 ± 5) min for LV function assessment were reported, which corresponds well to clinical imaging protocols at lower field strengths[21]. Thereby, spoiled gradient echo based CMR benefits from the prolonged $T_1$ relaxation times at ultra-high field that result in an enhanced blood-myocardium contrast superior to gradient echo imaging at 1.5 T. This renders subtle anatomic structures such as the pericardium, the mitral and tricuspid valves as well as the papillary muscles well identifiable. Congruously, spoiled gradient echo based cardiac chamber quantification at 7 Tesla agrees closely with LV parameters derived from 2D bSSFP CINE imaging at 1.5 T[20]. Apart from that, accurate right-ventricular (RV) chamber quantification was recently demonstrated feasible using a high resolution spoiled gradient echo sequence at 7 Tesla[29].

Recognizing the challenges and opportunities of CMR at ultra-high field, this work presents a setup and protocol customized for functional CMR acquisitions on an investigational 7 Tesla research scanner. The protocol outlines the technical underpinnings, shows how impediments can be overcome, and provides practical considerations that help to keep the extra experimental overhead at a minimum. The proposed imaging protocol constitutes a four-fold improvement in the spatial resolution *versus* today's clinical practice. It is meant to provide a guideline for clinical adaptors, physician scientists, translational researchers, application experts, MR radiographers, technologists and new entrants into the field.

## Protocol

The study is approved by the ethics committee of the University of Queensland, Queensland, Australia and informed consent has been obtained from all subjects included in the study.

## 1. Subjects

1. Recruit volunteer subjects over 18 years of age internally at the University of Queensland.
2. Informed consent
    1. Inform each subject about potential risks of undergoing the examination before entering the magnetic resonance imaging (MRI) safety zone. Specifically, discuss the ultra-high magnetic field exposure and possible contraindications for undergoing an MRI examination. Inform the subject that participating in the examination is voluntary and that at all times he/she may abort the examination. Obtain informed consent in writing.
    2. Explain the procedure to the participant. Since imaging is performed during breath hold at end expiration and consistent breath holding is integral to image quality, coach the subject on breathing technique prior to scanning.
    3. Perform MR safety screening on all subjects before entering the MRI safety zone in writing and again before entering the scanner room. Exclude subjects with contraindications for undergoing an MRI examination (*e.g.*, pacemakers, implanted defibrillators, other unsafe medical implants or claustrophobia).
3. Ask the subject to change into scrubs before entering the scanner room.

## 2. Preparation

1. Set up the additional hardware required to operate the dedicated 32 channel $^1$H cardiac transceiver (Tx/Rx) RF coil[26] on the patient table as outlined in **Figure 1a** and **b**. Apart from a small power splitter box (**Figure 1c**), the auxiliary coil equipment comprises one power splitter box and phase shifter box (**Figure 1d**) and one Tx/Rx interface box (**Figure 1e**) for each of the two RF coil sections that will be placed below and on top of the subject. The greater part it accommodates the local transmit electronics, which is required for signal excitation at 7 Tesla, since traditional birdcage body coils as commonly employed at 1.5 T and 3.0 T are not available.
2. Place the additional RF coil hardware at the top end of the patient table as outlined in **Figure 1b** and link the individual boxes together with the Bayonet Neill-Concelman (BNC) cables. Since the distance that the patient table can be driven into the MRI bore is limited, ensure to leave sufficient space on the patient table for the coil infrastructure to guarantee that the subject's heart can be positioned with the center of the coil at the isocenter of the magnet.
3. Connect the Tx/Rx interface boxes to the four coil plugs on the patient table.
4. Place the center of the posterior coil array 147 cm away from top end of the patient table (**Figure 1b**). This spot defines where the posterior coil array has to be placed to ensure that the subject's heart is at the isocenter of the magnet if the patient table is maximally driven into the bore. The placement on the predefined coil spot is crucial, to ensure optimal operation. Determine the optimal position of the posterior coil array as well as the positioning of the auxiliary equipment in preliminary tests including several volunteers of different body height.
5. Connect the four cables of the posterior coil array into the appropriate sockets of the Tx/Rx interface box for the posterior array.
6. Connect the four modules of the anterior coil array are with the Tx/Rx interface box for the top array and flip the array over the auxiliary coil equipment to allow for subject positioning.
7. Attach the three ECG electrodes to the body of the subject. Follow the vendor guidelines for electrode placement to ensure optimal operation of the system's trigger algorithm.
8. Position the subject on the patient table (**Figure 1f**). Critically, make sure that the subject's heart is positioned central to the posterior coil in order to guarantee scanning within the isocenter of the magnet. As, depending on the subject's height, the head will have to be placed on top of the coil/interface box connectors, place the cables carefully and use appropriate cushioning to ensure the subject's comfort and compliance.
9. Connect the trigger device to the ECG electrodes.
10. Attach the pulse trigger device to the subject's index finger. Use this second device for triggering in the event of severe distortions of the ECG signal introduced by the MHD effect.
11. Hand the safety squeeze ball to the subjects.
12. Equip the subject with headphones and earbuds to reduce the noise exposure and to allow communication with the subject.

13. Place the anterior coil on the subject's chest, such that the cables that connect to the plugs E-F and G-H are located to the right and left of the subject's head, respectively.
14. Drive the subject into the scanner bore. Perform the driving operation manually and ensure that the speed button of the table controls is in the off-position to guarantee the subject's safety during the driving process. Do not use the automatic mode as the variable table speed in this mode is optimized for neuro imaging and the distance the table can be driven automatically into the bore is limited by the scanner hardware.
15. Check if communication to the subject through the intercom is possible and if the subject is feeling well.
16. MR imaging
    1. Run basic localizer (scout) scans along the three physical gradient axes for slice planning and $B_0$-shimming.
    2. Use an ECG-triggered fast low angle shot (FLASH) sequence with the following acquisition parameters: field of view (FOV) = 400 mm, matrix = 192 x 144, slices per gradient axis = 1, thickness = 8 mm, echo time (TE) = 1.24, repetition time (TR) = 298 ms, flip angle = 10°.
    3. Apply parallel MRI with acceleration factor = 2, reference lines = 24 and generalized autocalibrating partially parallel acquisitions (GRAPPA) reconstruction.
    4. Use the localizer images to verify that the subject's heart is positioned in the isocenter of the magnet. Reposition the subject if necessary.

17. 3rd order B0-shimming
    1. Open the 3rd order shim tool (**Figure 2a**) and reset all 3rd order shim currents (**Figure 2b**).
    2. Prescribe the shim volume for proper shimming over a region covering the heart (**Figure 2c**).
    3. Run a non-triggered advanced flow compensated 2D multi-echo FLASH shim sequence for the calculation of the 3rd order shim currents. Use the following parameters: FOV = 400 x 400 mm, matrix = 80 x 80, slices = 64, thickness = 5.0 mm, TE1 = 3.06, TE2 = 5.10, TR = 7 ms, flip angle = 20 °, parallel MRI (GRAPPA), acceleration factor = 2, reference lines = 24.
    4. To calculate and apply the 3rd order shim currents, open the next protocol and copy the above-mentioned shim volume. Execute the **SetShim** program in the start menu (**Figure 2a**). Next, open the **Manual Adjustments** window in the **Options** menu (**Figure 2d**). In the **3D Shim** tab, click **Calculate | Apply** to set the shim currents for the 2nd order (**Figure 2e**). Finally, set the shim currents by clicking **Set Shim_3rd** in the 3rd order shim tool (**Figure 2b**).
    5. Close the **Manual Adjustments** window. Keep the shim volume and the shim currents fixed throughout the remainder of the examination. Note that the shimming procedure can be highly system specific.

18. Acquire further localizers to support double-oblique slice planning. Unless stated otherwise, use a breath held and ECG-triggered 2D FLASH sequence with the following parameters for all localizer measurements: FOV = 360 x 290 mm, matrix = 256 x 206, thickness = 6.0 mm, TE = 1.57, TR = 3.9 ms, flip angle = 35 °, parallel MRI (GRAPPA), acceleration factor: 2, reference lines: 24. Advise the patient to hold the breath in expiration. Employ high flip angles or use a segmented cine protocol (see below) to achieve improved contrast.
    1. Acquire the 2 chamber localizer (1 slice), planned perpendicular on the axial scout parallel to the septal wall (**Figure 3a**).
    2. Acquire the 4 chamber localizer (1 slice), planned perpendicular on the 2 chamber localizer slice through the mitral valve and the apex of the left ventricle (**Figure 3b**).
    3. Acquire the short axis localizer (7 slices, FOV = 360 x 330 mm), planned perpendicular on the 4 chamber localizer parallel to the mitral valve and perpendicular to the septal wall (**Figure 3c**).

19. Perform the CINE acquisitions. Use a high resolution breath held ECG-triggered segmented 2D FLASH sequence with the following parameters: FOV = 360 x 270 mm, matrix = 256 x 192/264 x 352, thickness = 4.0 mm, TE = 3.14, TR = 6.3 ms, flip angle = 35-55 °, segments = 7, parallel MRI (GRAPPA), acceleration factor = 2/3, temporal resolution = 42.6/44.3 ms.
    1. Start with the left ventricular 4 chamber view (horizontal long axis, HLA) slices. Plan the central slice through the center of the mitral and tricuspid valves and the apex of the left ventricle (**Figure 3d**). Acquire each slice within an individual breath hold in expiration.
    2. Next, acquire the left ventricular short axis slices. Plan them perpendicular to the HLA and parallel to the mitral valve so that it covers the whole left ventricle from the base to the apex (**Figure 3e**). To ensure accurate function testing, position the first slice accurately at the mitral valve leaflet insertions, so that the center of the slice is within the ventricle. Again, acquire each slice within an individual breath hold in expiration.

## Representative Results

Representative results of cardiac CINE examinations derived from volunteers are depicted in **Figure 4**. Shown are diastolic and systolic time-frames of short axis and a four-chamber long axis views of the human heart. The significantly higher spatial resolution for the short axis views (**Figure 4a**, **4b, 4e**, **4f**) compared to the long axis views (**Figure 4c**, **4d**, **4g**, **4h**) is clearly visible. In both short and long axis slices, the images provide ample signal-to-noise and blood-myocardium contrast to clearly delineate the myocardial walls, even when employing a slice thickness as thin as 4 millimeters. The employed parallel imaging acceleration scheme reconstructed the images with high image quality and without conspicuous noise enhancement.

Due to R-wave recognition failure of the ECG, pulse oximetry-based triggering was utilized for the image acquisitions on the right (**Figure 4e**-**4h**). The jitter in the pulse oximetry signal peak induced minor motion artifacts which were pronounced during periods of cardiac contraction and relaxation as highlighted in the long axis view shown in **Figure 4h** (red arrow). Signal voids due to destructive interferences in the transmission field are marked by yellow arrows.

Typical ECG signals obtained in one channel of the trigger device in one healthy subject are depicted in **Figure 5**. When comparing the ECG signal acquired outside of the magnet bore (**Figure 5a**) to the one obtained with the subject positioned at the isocenter of the magnet (**Figure 5b**), significant differences become evident. Within the ultra-high magnetic field, the ECG signal is severely corrupted by the MHD effect. The adverse phenomenon arises from the interaction between the conductive fluid blood with the external magnetic field. It induces a distorting electric field superimposing the heart's own depolarization fields and thus corrupts the signal picked up by ECG electrodes on the subject's skin. The MHD effect scales with B0 and is particularly pronounced during cardiac phases of systolic aortic flow, which is why mainly the S-T segment of the ECG signal is affected. Although the R-wave of the ECG signal is typically not directly affected, it can impair the R-wave recognition and cardiac synchronization. It is noteworthy that, due to the ECG signal distortions, ECG signals obtained in the presence of high magnetic fields cannot be used as a patient emergency condition indicator. A representative pulse signal obtained inside of the magnet bore is displayed in **Figure 5c**. The pulse signal is not affected by the magnetic field. The delay of the pulse wave to the R-wave at 0 ms, which can introduce artifacts, is clearly visible.

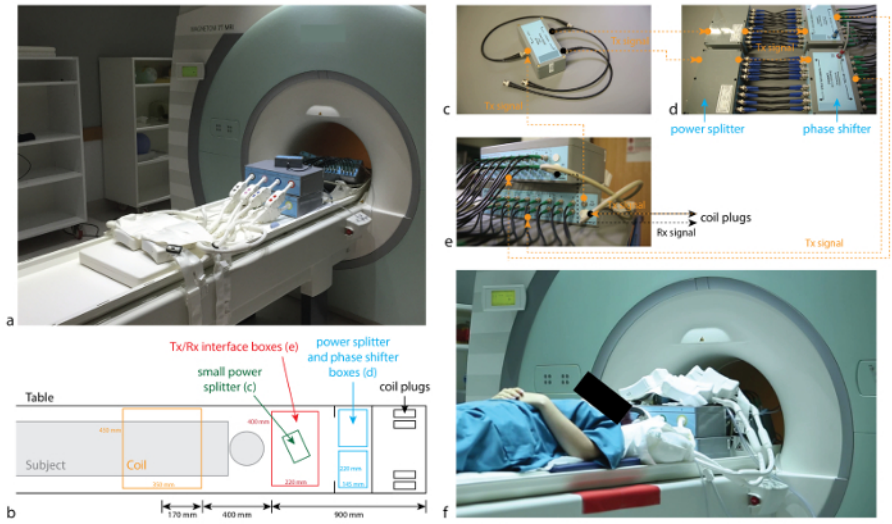


**Figure 1: Experimental setup and elements of the 32 channel cardiac Tx/Rx coil and coil hardware.** (a, b) The auxiliary hardware consisting of 7 hardware boxes and connecting BNC cables is placed at the top end of the patient table in order provide as much space as possible for subject positioning. The posterior and anterior coil elements are connected with eight cables to the interface boxes. For the system at hand, the posterior coil array is placed no further than 1470 mm from the top end of the table, to ensure positioning of the heart at the isocenter of the magnet. (c) small power splitter box. (d) one power splitter and phase shifter box each for the posterior and anterior coil array. (e) Tx/Rx interface boxes for the anterior (top) and posterior (bottom) coil array. Orange and black dotted arrows indicate transmit (Tx) and receive (Rx) signal pathways. (f) Subject positioned on the posterior coil array. The head rests on a cushion on the 8 coil connectors. The predefined coil spot is marked with a red label. Please click here to view a larger version of this figure.


**Figure 2: 3rd order shimming using the systems adjustment and shim tools.** (a) Start menu with buttons for the "3rd order shim" tool and "set shim" program. (b) "3rd order shim" tool. (c) Positioning of the adjustment region over the heart. (d) Starting the "Adjustments" tool from the "Options" menu. (e) "Adjustments" tool with buttons to calculate and apply the 2nd order shim currents in the "3D shim" tab. Please click here to view a larger version of this figure.

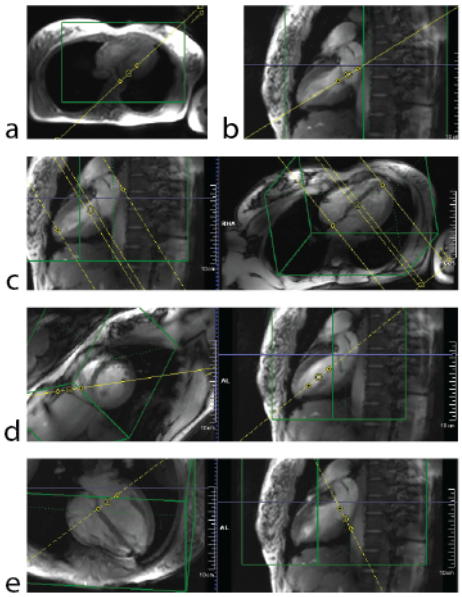


**Figure 3: Slice planning for cardiac CINE imaging.** (a) planning of 2-chamber localizer perpendicular on basic localizer. (b) planning of 4 chamber localizer perpendicular on 2 chamber localizer (c) planning of short axis localizer on 2 chamber localizer (left) and perpendicular on 4 chamber localizer (right). (d) planning of left ventricular 4 chamber view perpendicular on short axis localizer (left) and on 2 chamber localizer (right). (e) planning of left ventricular short axis slices on left ventricular 4 chamber view (left) and 2 chamber localizer (right).

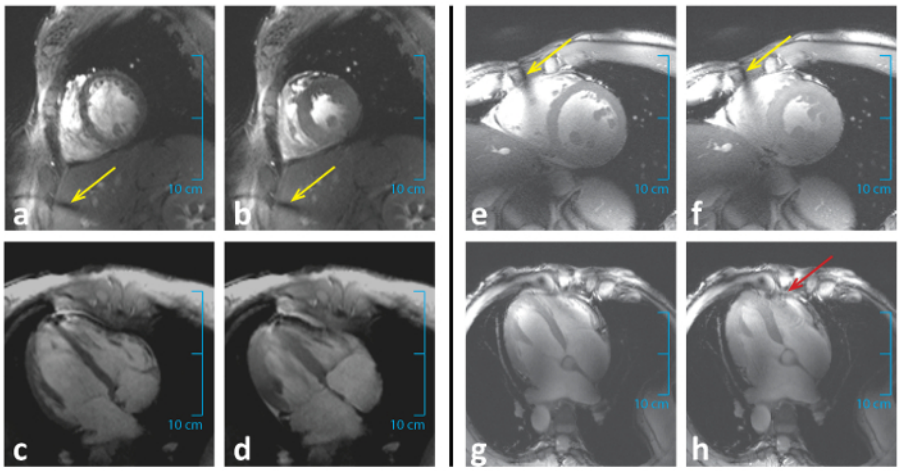


**Figure 4: Representative results of high resolution cardiac CINE imaging in two subjects using ECG triggering (a-d) and pulse triggering (e-h).** (a, e) End-diastolic time frames of a mid-ventricular short axis slice acquired with a spatial resolution of 1.0 x 1.0 x 4 $mm^3$. (b, f) Corresponding end-systolic time frames. (c, g) End-diastolic time frames of a horizontal long axis slice. (d, h) Corresponding end-systolic time frames. Signal dropouts caused by RF field non-uniformities are marked by yellow arrows. Slight trigger errors caused by the latency of the pulse wave are depicted in the long axis view of the pulse-triggered scan (red arrow). Please click here to view a larger version of this figure.

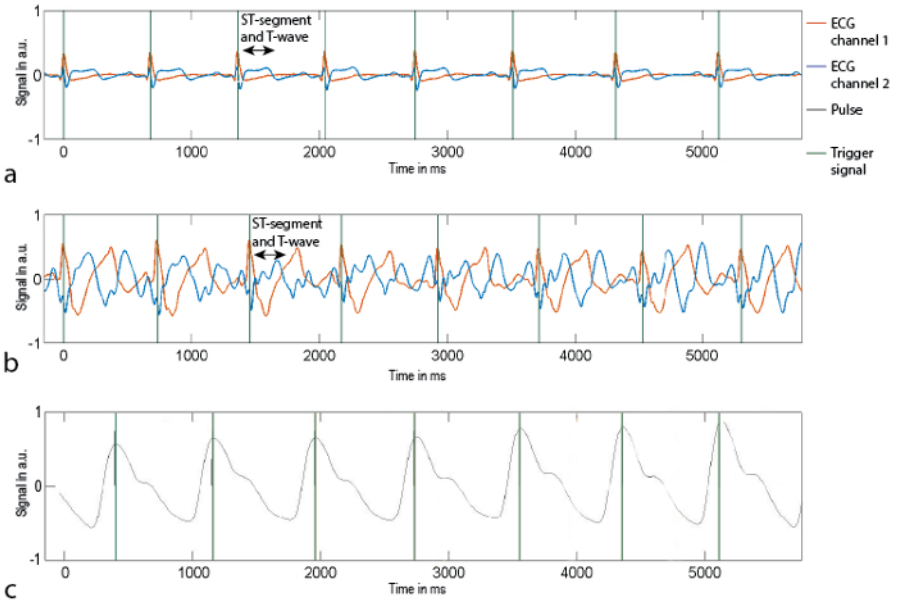


**Figure 5: Representative ECG signals obtained outside and inside of the magnet bore at 7 Tesla.** (a) ECG signal obtained in the two channels (red, blue) of the ECG trigger device outside of the magnet bore. The R-wave can be clearly distinguished. Trigger events are demarcated in green. (b) ECG signal obtained at the isocenter of the 7 Tesla magnet bore. The MHD effect clearly affects the ECG signal and particularly the S-T element of the ECG signal. The strong signal fluctuations can lead to mis-triggering. (c) Representative pulse signal obtained at the isocenter of the 7 Tesla magnet bore for comparison. The pulse signal is not affected by the magnetic field. Note that the pulse wave is delayed with respect to the ECG R-wave. Please click here to view a larger version of this figure.

## Discussion

Functional CMR examinations could be conducted successfully at 7 Tesla. Based on the field strength driven SNR gain, CINE images of the human heart could be acquired with significantly higher spatial resolution compared to 1.5 or 3 T. While a slice thickness of 6 to 8 mm and in-plane voxel edge lengths of 1.2 to 2.0 mm are commonly used at lower clinical field strengths[1,30], the measurements at 7 Tesla could be conducted with a slice thickness of 4 mm and an isotropic in-plane resolution of 1.0 mm.

The results obtained at 7 Tesla are promising. The image quality is comparable to that obtained at 1.5 T or 3 T although $B_1$+ shimming was not conducted and the experimental overhead was kept to a minimum to facilitate clinically acceptable examination times for cardiac chamber quantification. Occasionally image quality was slightly impaired by signal voids caused by focal RF field non-uniformities. In these cases, the use of $B_1$+ shimming, which is available through parallel transmission techniques might be beneficial. While this approach is tempting and looming on the horizon of clinical applications it requires further considerations on signal absorption rate (SAR) management.

On the triggering side, the ECG signal was occasionally severely corrupted by the MHD effect so that synchronization of image acquisition with the cardiac activity needed to be conducted using the pulse triggering approach. When using the pulse trigger, slight impairment of the CINE image quality may occur. This impairment is caused by the time the pulse trigger is delayed with respect the R-wave of the ECG. Variations and jitter in the pulse trigger signal can range up to 60 milliseconds. This phenomenon may lead to mis-triggering and may risk introducing cardiac motion induced blurring in the reconstructed images. As recently demonstrated, accurate cardiac synchronization at 7 Tesla can be achieved by fully exploiting the technical capabilities of available trigger devices and by using state-of-the art trigger algorithms[19,24]. Besides this, the use of alternative triggering solutions[31,32,33] may also provide a good basis for synchronized imaging.

Scanning at ultra-high-field comes along with a significantly increased demand of hardware. In particular the scan preparations are more complex *versus* lower field strengths. This can be attributed to the use of auxiliary RF coil equipment due to the absence of a body coil that is integrated in clinical scanners. Subject positioning requires more care *versus* the routine clinical setup at lower field strengths, since not only the subject comfort but also the position of the coil with respect to the table has to be taken into account. This limitation is related to the design and the capabilities of today's patient tables for 7 Tesla MRI but is expected to be fixed with the ongoing move to the next generation of 7 Tesla MRI systems. Only recently, the first 7 Tesla MRI system was approved for clinical use for specific applications in the USA and Europe. Experimental overhead is also introduced by the MHD effect that can severely impair the R-wave recognition. To ensure a good cardiac synchronization, a careful subject preparation, an accurate ECG electrode placement in addition to an accurate calibration of the ECG trigger algorithm are required[24]. In some cases, repositioning of the ECG electrodes after moving the subject into the bore might become necessary. Also, to ensure the continuation of the examination in the presence of severe ECG trigger impairments, it is advisable to attach the pulse trigger device to the subject. As an alternative to ECG triggering, acoustic triggering[31] might be utilized, which is immune to MHD effects and has been shown to be superior to pulse triggering. If these considerations and measures are carefully included into functional CMR examinations at 7 Tesla, the workflow and duration of cardiac CINE measurements at ultra-high fields is similar to that at clinical field strengths.

The increasing use of ultra-high field systems in translational research will advance the capabilities of CMR for the assessment of cardiovascular diseases. Technological advances such as improved RF coil technology or multi-transmit MR systems will help to reduce the current

experimental overhead and streamline additional scan preparations and shimming operations. Within this context, a careful validation of the novel ultra-high field CMR applications against the well-established CMR applications at 1.5 T or 3 T will be essential.

This study demonstrates, that functional CMR examinations can be successfully conducted at 7 Tesla. The field strength driven SNR gain at ultra-high field allows for CINE acquisitions with very high spatial resolutions. Compared to the clinical field strengths of 1.5 or 3 Tesla, the spatial resolution can be increased by a factor of 3 to 4. The experimental overhead required to tackle the various technical challenges can be kept to a minimum. These results as well as future technological developments will provide the basis for explorations into more advanced applications such as myocardial tissue characterization, metabolic imaging or microstructure imaging.

## Disclosures

Kieran O'Brien and Jonathan Richer are employed by Siemens Ltd. Australia. Jan Rieger and Thoralf Niendorf are founders of MRI.TOOLS GmbH, Berlin, Germany. Jan Rieger was CTO and an employee of MRI.TOOLS GmbH. Thoralf Niendorf is CEO of MRI.TOOLS GmbH.

## Acknowledgements

The authors acknowledge the facilities, and the scientific and technical assistance of the National Imaging Facility at the Centre for Advanced Imaging, University of Queensland. We would also like to thank Graham Galloway and Ian Brereton for their help to obtain a CAESIE grant for Thoralf Niendorf.

## References

1. Kramer, C.M., *et al.* Standardized cardiovascular magnetic resonance (CMR) protocols 2013 update. *Journal of Cardiovascular Magnetic Resonance.* **15** (1), 1 (2013).
2. Earls, J.P., Ho, V.B., Foo, T.K., Castillo, E., Flamm, S.D. Cardiac MRI: Recent progress and continued challenges. *Journal of Magnetic Resonance Imaging.* **16** (2), 111-127 (2002).
3. Wintersperger, B.J. *et al.* Cardiac CINE MR imaging with a 32-channel cardiac coil and parallel imaging: Impact of acceleration factors on image quality and volumetric accuracy. *Journal of Magnetic Resonance Imaging.* **23** (2), 222-227 (2006).
4. Schmitt, M. *et al.* A 128-channel receive-only cardiac coil for highly accelerated cardiac MRI at 3 Tesla. *Magnetic Resonance in Medicine.* **59** (6), 1431-1439 (2008).
5. Wech, T. *et al.* High-resolution functional cardiac MR imaging using density-weighted real-time acquisition and a combination of compressed sensing and parallel imaging for image reconstruction. *RöFo: Fortschritte Auf Dem Gebiete Der Röntgenstrahlen Und Der Nuklearmedizin.* **182** (8), 676-681 (2010).
6. Stäb, D. *et al.* CAIPIRINHA accelerated SSFP imaging. *Magnetic Resonance in Medicine.* **65** (1), 157-164 (2011).
7. Gutberlet, M. *et al.* Influence of high magnetic field strengths and parallel acquisition strategies on image quality in cardiac 2D CINE magnetic resonance imaging: comparison of 1.5 T *vs.* 3.0 T. *European Radiology.* **15** (8), 1586-1597 (2005).
8. Gutberlet, M. *et al.* Comprehensive cardiac magnetic resonance imaging at 3.0 Tesla: feasibility and implications for clinical applications. *Investigative radiology.* **41** (2), 154-167 (2006).
9. Kraff, O., Fischer, A., Nagel, A.M., Mönninghoff, C., Ladd, M.E. MRI at 7 tesla and above: Demonstrated and potential capabilities: Capabilities of MRI at 7T and Above. *Journal of Magnetic Resonance Imaging.* **41** (1), 13-33 (2015).
10. Moser, E., Stahlberg, F., Ladd, M.E., Trattnig, S. 7-T MR-from research to clinical applications? *NMR in Biomedicine.* **25** (5), 695-716 (2012).
11. Hecht, E.M., Lee, R.F., Taouli, B., Sodickson, D.K. Perspectives on Body MR Imaging at Ultrahigh Field. *Magnetic Resonance Imaging Clinics of North America.* **15** (3), 449-465 (2007).
12. Niendorf, T. *et al.* W(h)ither human cardiac and body magnetic resonance at ultrahigh fields? technical advances, practical considerations, applications, and clinical opportunities: Advances in ultrahigh field Cardiac and Body Magnetic Resonance. *NMR in Biomedicine.* **29** (9), 1173-1179 (2016).
13. Niendorf, T., Sodickson, D.K., Krombach, G.A., Schulz-Menger, J. Toward cardiovascular MRI at 7 T: clinical needs, technical solutions and research promises. *European Radiology.* **20** (12), 2806-2816 (2010).
14. Niendorf, T. *et al.* Progress and promises of human cardiac magnetic resonance at ultrahigh fields: A physics perspective. *Journal of Magnetic Resonance.* **229**, 208-222 (2013).
15. Hinton, D.P., Wald, L.L., Pitts, J., Schmitt, F. Comparison of Cardiac MRI on 1.5 and 3.0 Tesla Clinical Whole Body Systems: *Investigative Radiology.* **38** (7), 436-442 (2003).
16. Ohliger, M.A., Grant, A.K., Sodickson, D.K. Ultimate intrinsic signal-to-noise ratio for parallel MRI: Electromagnetic field considerations. *Magnetic resonance in medicine.* **50** (5), 1018-1030 (2003).
17. Vaughan, J.T. *et al.* Whole-body imaging at 7T: Preliminary results. *Magnetic Resonance in Medicine.* **61** (1), 244-248 (2009).
18. Hezel, F., Thalhammer, C., Waiczies, S., Schulz-Menger, J., Niendorf, T. High Spatial Resolution and Temporally Resolved T2* Mapping of Normal Human Myocardium at 7.0 Tesla: An Ultrahigh Field Magnetic Resonance Feasibility Study. *PLOS ONE.* **7** (12), e52324 (2012).
19. Suttie, J.J. *et al.* 7 Tesla (T) human cardiovascular magnetic resonance imaging using FLASH and SSFP to assess cardiac function: validation against 1.5 T and 3 T. *NMR in biomedicine.* **25** (1), 27-34 (2012).
20. Knobelsdorff-Brenkenhoff, F. *et al.* Cardiac chamber quantification using magnetic resonance imaging at 7 Tesla-a pilot study. *European Radiology.* **20** (12), 2844-2852 (2010).
21. Winter, L. *et al.* Comparison of three multichannel transmit/receive radiofrequency coil configurations for anatomic and functional cardiac MRI at 7.0T: implications for clinical imaging. *European Radiology.* **22** (10), 2211-2220 (2012).
22. Schmitter, S. *et al.* Cardiac imaging at 7 tesla: Single- and two-spoke radiofrequency pulse design with 16-channel parallel excitation: Cardiac Imaging at 7T. *Magnetic Resonance in Medicine.* **70** (5), 1210-1219 (2013).
23. Krug, J., Rose, G., Stucht, D., Clifford, G., Oster, J. Limitations of VCG based gating methods in ultra high field cardiac MRI. *Journal of Cardiovascular Magnetic Resonance.* **15** (Suppl 1), W19 (2013).

 

24. Stäb, D., Roessler, J., O'Brien, K., Hamilton-Craig, C., Barth, M. ECG Triggering in Ultra-High Field Cardiovascular MRI. *Tomography.* **2** (3), 167-174 (2016).
25. Gräßl, A. *et al.* Design, evaluation and application of an eight channel transmit/receive coil array for cardiac MRI at 7.0T. *European Journal of Radiology.* **82** (5), 752-759 (2013).
26. Graessl, A. *et al.* Modular 32-channel transceiver coil array for cardiac MRI at 7.0T. *Magnetic Resonance in Medicine.* **72** (1), 276-290 (2014).
27. Snyder, C.J. *et al.* Initial results of cardiac imaging at 7 tesla. *Magnetic Resonance in Medicine.* **61** (3), 517-524 (2009).
28. Meloni, A. *et al.* Detailing magnetic field strength dependence and segmental artifact distribution of myocardial effective transverse relaxation rate at 1.5, 3.0, and 7.0 T: Magnetic Field Dependence of Myocardial $R_2$*. *Magnetic Resonance in Medicine.* **71** (6), 2224-2230 (2014).
29. von Knobelsdorff-Brenkenhoff, F. *et al.* Assessment of the right ventricle with cardiovascular magnetic resonance at 7 Tesla. *Journal of Cardiovascular Magnetic Resonance.* **15**, 23 (2013).
30. Petersen, S.E. *et al.* Reference ranges for cardiac structure and function using cardiovascular magnetic resonance (CMR) in Caucasians from the UK Biobank population cohort. *Journal of Cardiovascular Magnetic Resonance.* **19** (1) (2017).
31. Frauenrath, T. *et al.* Feasibility of cardiac gating free of interference with electro-magnetic fields at 1.5 Tesla, 3.0 Tesla and 7.0 Tesla using an MR-stethoscope. *Investigative radiology.* **44** (9), 539-547 (2009).
32. Frauenrath, T. *et al.* Acoustic cardiac triggering: a practical solution for synchronization and gating of cardiovascular magnetic resonance at 7 Tesla. J*ournal of Cardiovascular Magnetic Resonance.* **12** (1), 67 (2010).
33. Schroeder, L. *et al.* A Novel Method for Contact-Free Cardiac Synchronization Using the Pilot Tone Navigator. *Proceedings of the International Society for Magnetic Resonance in Medicine.* **24**, 3103 (2016).


 